BJR

Received: 18 August 2015 | Revised: 13 October 2015 | Accepted: 16 November 2015

doi: 10.1259/bjr.20150687

Cite this article as:
Nardi C, Molteni R, Lorini C, Taliani GG, Matteuzzi B, Mazzoni E, et al. Motion artefacts in cone beam CT: an *in vitro* study about the effects on the images. *Br J Radiol* 2016; **89**: 20150687.

FULL PAPER

Motion artefacts in cone beam CT: an *in vitro* study about the effects on the images

[1]COSIMO NARDI, MD, [2]ROBERTO MOLTENI, PhD, [3]CHIARA LORINI, PhD, [1]GIAN G TALIANI, MD, [1]BENEDETTA MATTEUZZI, MD, [1]ELISA MAZZONI, MD and [1]STEFANO COLAGRANDE, MD

[1]Department of Experimental and Clinical Biomedical Sciences, Radiodiagnostic Unit n. 2, University of Florence—Azienda Ospedaliero-Universitaria Careggi, Florence, Italy
[2]Arlington Heights, IL, USA
[3]Department of Health Science, University of Florence, Florence, Italy

Address correspondence to: Dr Cosimo Nardi
E-mail: *cosimo.nardi@unifi.it*

Objective: In cone beam CT (CBCT), imperfect patient immobility, caused by involuntary movements, is one of the most important causes of artefacts and image quality degradation. Various works in literature address this topic, but seldom is the nature of the movement correlated with the type of artefact and the image degradation in a systematic manner, and the correlation analyzed and explained.
Methods: All three types of movements that can occur during a scan—nodding, tilting and rolling—were applied to a dry skull, in various manners from abrupt to gradual through the entire scan, at different times and angles, over a wide range of displacements. 84 scans were performed, with different skull movements, and the resulting images examined by two skilled radiologists, rated in a four-point scale and statistically analyzed. A commercial CBCT machine was used, featuring supine patient positioning.
Results: Different types of movements induce different artefacts, in different parts of the anatomy. In general, movement of short duration may lead to double contours (bilateral or monolateral depending upon the angle of the scan at which they occur), whereas gradual movements result into blurring.
Conclusion: Not all movements cause motion artefacts that equally jeopardize the image. Rolling is the type of movement that most severely affects the image diagnostic value.
Advances in knowledge: These findings may help practitioners to identify the causes of motion artefacts and the resulting image degradation, and remediate them, and manufacturers to improve the patient-positioning devices.

INTRODUCTION

Cone beam CT (CBCT) devices have a long acquisition time, ranging from 5.4 to 40 s,[1] and such a time is long enough for motion artefacts, caused by patient's movements, to be significant. In fact, approximately 21–42% of the *in vivo* examinations exhibit motion artefacts.[2,3] Recently, several works have been published in the literature about movements in dental and maxillofacial CBCT,[2–10] but correlation between the various possible movements and the resulting different kinds of artefacts, which may be induced, is lacking.

New-generation CBCT systems employ flat-panel detectors, but since large-area flat-panels are expensive, the manufacturer sometimes uses a smaller detector and offsets the source-to-rotation-centre axis with respect to the centre of the detector. That allows capturing data from a larger anatomical volume with respect to an axially centred detector.[11]

Volumetric reconstructions in both classic CT and CBCT is usually performed *via* a back-projection process, in which all the acquired information (two-dimensional projection images in case of CBCT) equally contribute to the reconstruction of the volume. In CBCT, back-projection is implemented *via* mathematical algorithms, such as that of Feldkamp, Davis and Kress (FDK), that remediate the non-ideal geometrical conditions.[12,13] This process requires that the patient remains immobile during the entire acquisition. Correction algorithms to compensate for possible (small) movements and to limit the formation of motion artefacts have not yet been implemented.[5,10] CT (single slice and multislice) and CBCT differ in voxel size (0.5–1 mm in CT vs 0.075–0.4 mm in CBCT), in the geometry (narrow-pyramid or fan beam in CT vs wide-pyramid or cone beam in CBCT), in radiation load (40–120 mA in CT vs 1–20 mA in CBCT), in tube potential (80–150 kV in CT vs 40–120 kV in CBCT) and in detector shape (one-dimensional in CT *vs* two-dimensional in CBCT). These differences produce either artefacts typical of

Figure 1. Arrangement allowing the dry skull movement by shifting the pole.

each technology[5,14,15] or cause the same type of artefact to manifest in a different way.[5,16,17]

The aim of this study is to evaluate type, severity, area and extension of artefacts caused in CBCT by small movements (motion artefacts), applied to a dry skull, in order to determine the reasons of image deterioration, and to verify the conditions in which motion artefacts do not visually impair the images. This may lead to new technical solutions to reduce the number of retakes and consequently the overall radiation load to patients.

METHODS AND MATERIALS

Device

Scans were performed by a cone beam CT system (NewTom™ 5G; QR srl, Verona, Italy), equipped with amorphous silicon flat-panel detector (20 × 25 cm). The reconstructed images were observed with a medical monitor, 3 MegaPixel Barco display, 20-inch, 2048 × 1536 resolution (Barco, Kortrijk, Belgium). In NewTom 5G, the patient is positioned supine, contrarily to most other commercial CBCT machines where the patient sits or stands upright. X-ray tube rotation is counter clockwise, starting at 12 o'clock. Therefore:

(1) 0° vertical X-ray beam, X-ray source at the top
(2) 90° horizontal X-ray beam, X-ray source on the right
(3) 180° vertical X-ray beam, X-ray source at the bottom
(4) 270° horizontal X-ray beam, X-ray source on the left.

The same field of view (FOV; 12 × 8 cm) and the same protocol were used for all examinations. The protocol is called "Hi-Res Regular" by the producer: scan time 26 s, effective current–time product 4.5 mAs, 110 kV, beam angle 12.4°, number of acquired images 360 (13.85 images s^{-1}). The software originally provided with the system was utilized for image evaluation. No other software was used to prevent additional errors from reconstruction interpolation. All CBCT volumes were reconstructed with 150 μm isometric voxel size.

System development and dry skull

A whole dry skull, complete with all head bones, including teeth, and free from oral metallic therapy, was used. To keep the mouth closed, the mandible was blocked by two springs (one for each side) fixed to the temporal bone and coronoid process. The skull cap was dissected on the axial plane at the frontal–occipital level to permit access inside.

A round wooden pole (length 2.4 m and diameter 2.3 cm) was inserted in the skull through the foramen magnum and secured on the skull vertex with a screw, so that the occlusal plane was perpendicular to the pole. It was laid on a wooden block at a distance of 2 m, in which limit stops were inserted to allow accurate amplitude of the nodding, tilting and rolling movements (Figures 1 and 2).

Head and pole movements

The pole motion caused movements of various amplitude in different anatomic skull areas. Soft gradual movements were performed to reproduce the action *in vivo* as far as possible. The

Figure 2. The three types of imparted movement: nodding, tilting and rolling.

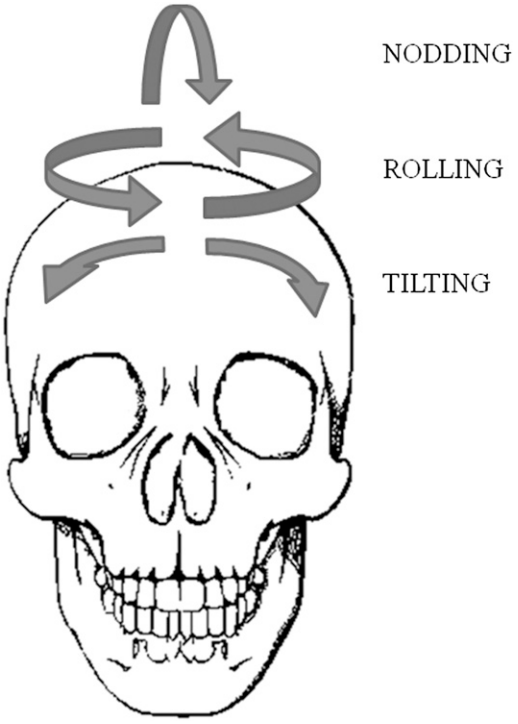

anatomic landmarks were: upper central incisor occlusal surface (I), zygomatic-temporal suture (Z) and mandible angle (M) (Figure 3). The I, Z and M resulting movement was determined either mathematically or by CAD three-dimensional (3D) Autodesk Inventor® software (http://usa.autodesk.com/autodesk-inventor/) (Table 1). The fulcrum was the skull vertex in rolling and the occiput in tilting and nodding.

Movement parameters:
(1) *Modality*: manual, by two trained operators
(2) *Type*: tilting, nodding, rolling
(3) *Shift*: tilting and nodding: 2.5, 5, 10 cm; rolling: 3°; I, Z and M: variable from 0.5 to 9.6 mm
(4) *Start time*: variable from 0 to 26 s. After 6.5, 13, 19.5 s, the X-ray source is at 90°, 180°, 270°, respectively
(5) *Duration*: variable from 1/4 to 26 s, corresponding at a rapid 2.5 cm shift and a complete rotation time, respectively
(6) *Velocity*: 10 cm s^{-1} (assisted by a stopwatch and a metronome).

Tilting and nodding were obtained by moving the pole 2.5, 5 and 10 cm between two limit stops secured on a wooden block, in the horizontal and vertical directions, respectively.

Rolling 3° was obtained by rotating the pole with a handle placed between two limit stops secured on the same wooden block.

Movement type

2 m away from the skull vertex, 3° pole rotation and 2.5-, 5-, 10-cm pole tilting and nodding were effected. The 12 following types of movements were carried out:
(1) Rapid (abrupt): after 6.5, 13 and 19.5 s
(2) 2-s continuous: between 5.5 and 7.5; 12 and 14; and 18.5 and 20.5 s
(3) 6-s continuous: between 3.5 and 9.5; 10 and 16; and 16.5 and 22.5 s
(4) 13-s continuous: between 0 and 13, and 13 and 26 s
(5) 26-s continuous: between 0 and 26 s.

The total number of scans was 84 (tilting 36, nodding 36, rolling 12), allotted as follows:
(1) 12 tilting each of 2.5, 5 and 10 cm
(2) 12 nodding each of 2.5, 5 and 10 cm
(3) 12 rolling of 3°.

Operators and observers

The procedures were carried out by two operators coached until an excellent reproducibility of pole movement was achieved. They took advantage of a stopwatch (for the start and the end) and a metronome (for the rhythm) for time consistency of the movements.

The operators wore radiation protective clothing and stood 2.5 m away from the X-rays source. The surrounding environment was protected by leaded shields, which entirely covered the gantry except a hole for the pole access.

Two independent observers with dental imaging experience (20 and 9 years', respectively) evaluated all the outcomes from the procedures separately.

Image evaluation

Artefacts were evaluated in the axial, panoramic, cross, coronal and sagittal sections by:
(1) Severity index, divided into four tiers:
- G0: absence
- G1: no significant presence. An excellent image analysis is achievable
- G2: significant presence. A diagnostic image analysis is possible
- G3: remarkable presence. A reliable opinion cannot be formulated

(2) Area: anatomical region where the artefact is located. The general evaluation was carried out considering all the four quadrants in which the dental arches are conventionally divided. The particular evaluation was performed by

Figure 3. Anatomic landmarks and their projection on the pole centre. Vertex (v), occiput (o) and its projection (*o*); upper central incisor occlusal surface (I) and its projection (*i*); zygomatic-temporal suture (Z) and its projection (*z*); and mandible angle (M) and its projection (*m*). Distance *o*–v: 8 cm; distance *i*–v: 11.5 cm; distance *z*–v: 9 cm; distance *m*–v: 14 cm; distance *o*–o: 7.5 cm (sagittal plane) and 0 cm (frontal plane); distance *i*–I: 11.5 cm (sagittal plane), 0 cm (frontal plane); distance *z*–Z: 6 cm (sagittal plane), 5.5 cm (frontal plane); distance *m*–M: 4 cm (sagittal plane), 4 cm (frontal plane).

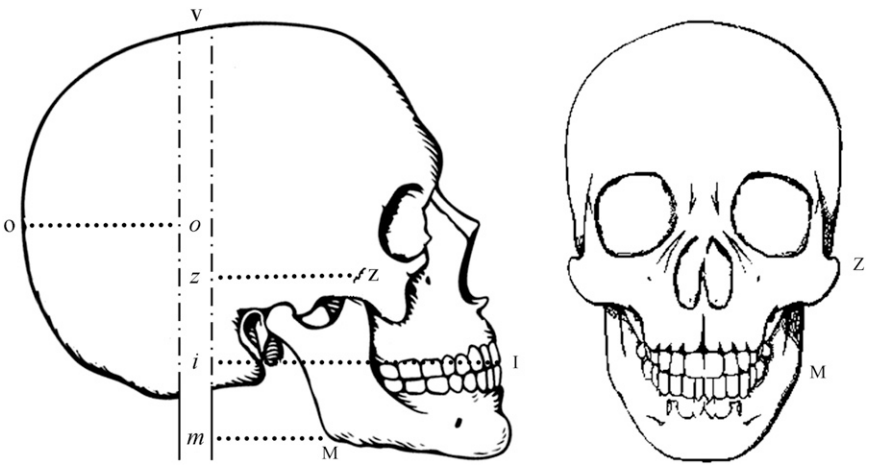

Table 1. Movement of upper central incisor (I), zygomatic-temporal suture (Z) and mandible angle (M), obtained by trigonometric calculation (TC) and AutoCAD simulation software (AC) (http://usa.autodesk.com/autodesk-inventor/), ensuing from 2.5-, 5- and 10-cm pole tilting and nodding movements and 3° pole rolling movement

Anatomical point	Tilting						Nodding						Rolling			
	2.5-cm		5-cm		10-cm		2.5-cm		5-cm		10-cm		3°			
	TC (mm)	AC (mm)	TC (mm)	AC (mm)	TC (mm)	AC (mm)	TC (mm)	AC (mm)	TC (mm)	AC (mm)	TC (mm)	AC (mm)	TC (mm)	AC (mm)		
I	0.5	0.456	0.9	0.912	1.8	1.823	2.4	2.398	4.8	4.796	9.6	9.592	6.0	6.018		
Z	0.9	0.899	1.8	1.798	3.6	3.597	1.7	1.701	3.4	3.403	6.8	6.806	3.1	3.140		
M	1.3	1.299	2.6	2.598	5.2	5.196	1.5	1.458	2.9	2.915	5.8	5.830	2.1	2.120		

focusing on the anatomical area (2 × 2 cm) corresponding to the I, Z and M points
- Quadrant I: upper arch, right side
- Quadrant II: upper arch, left side
- Quadrant III: lower arch, left side
- Quadrant IV: lower arch, right side

(3) Extension:
- True monolateral artefact: artefact displayed on one or both quadrants on one side only (Figure 4)
- False monolateral artefact: artefact displayed at least on one quadrant per side. The sum of the severity indexes of the quadrants of one side is greater than the double of the sum of the counter lateral side: (I + IV) > 2 (II + III) and *vice versa* (Figure 5)
- Bilateral artefact: artefact displayed at least on one quadrant per side. The sum of the severity indexes of the quadrants of one side is less or equal to the double of the sum of the counter lateral side: (I + IV) ≤ 2 (II + III) and *vice versa*) (Figures 6 and 7)

Obviously, in all the cases in which one side is artefact free (true monolateral artefact), no sums were used.

(4) Artefact type: smearing, double contour, cancellous bone fading (loss of trabeculae visibility) and general unsharpness.

Statistical analysis

Collected data were analyzed using the SPSS® v. 22.0 statistical analysis software (IBM Corp., New York, NY; formerly SPSS Inc., Chicago, IL).

For each anatomical region and each anatomic landmark, the agreement between observers in the evaluation of the images was assessed by using Cohen's kappa (k ≤ 0.39, poor agreement; k = 0.40–0.59, fair agreement; k = 0.60–0.74, good agreement; k ≥ 0.75, excellent agreement; a *p*-value ≤0.05 was considered as statistically significant). The observers compared the discordant evaluations and reached a consensus. The final database was composed of the evaluations arising from the agreement between the two observers. Data were reported as percentage values.

Figure 4. True monolateral artefact. Lower jaw cone beam CT axial section originated by a rapid tilting movement of 10 cm, at 19.5 s. The artefacts, in particular, the double contour, affect solely and entirely the mandible right side. The mandible left side is free from artefacts.

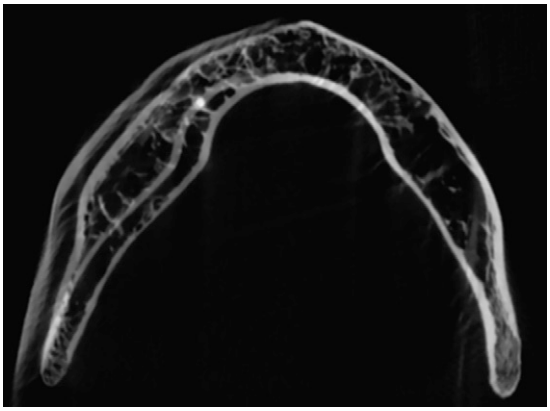

Figure 5. False monolateral artefact. Upper jaws cone beam CT axial section originated by a continuous rolling movement lasting 2 s (5.5–7.5 s). The artefacts, in particular the smearing, affect mainly the anterior anatomical region of the left jaw (short artefact).

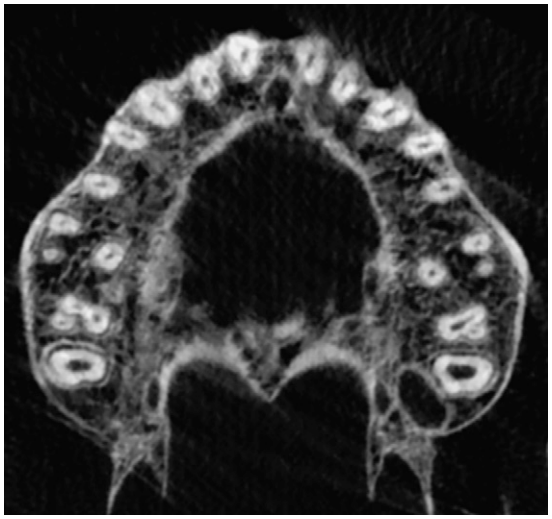

RESULTS

The agreement between the two observers was good, with kappa values ranging from 0.60 to 0.74 ($p < 0.01$).

The overall evaluation of all quadrants and anatomic landmarks showed artefacts in 82% of the examinations. The remaining 18%, *i.e.*, the cases where all values are in the G0 tier, was related to 2.5-cm tilting movements in 12% of the cases, 5-cm tilting in 2% of cases and 2.5-cm nodding in 4% of cases.

Figure 6. Bilateral artefact. Upper and lower jaws, cone beam CT coronal section originated by a nodding continue movement of 2.5 cm lasting 13 s. All the types of artefact are very obvious and affect both upper and lower jaws. The artefacts appear in the craniocaudal direction.

Figure 7. Bilateral artefact. Upper and lower jaws, cone beam CT coronal section originated by a tilting continue movement of 5 cm lasting 13 s. All the types of artefact are very obvious and affect both the upper and lower jaws. The artefacts appear in the buccolingual direction.

The artefacts' prevalence depended on:

Extent of pole displacement: 10 cm = 100%, 5 cm = 92%, 2.5 cm = 46%

Type of movement: tilting = 67%, nodding = 92%, rolling = 100%

Duration of movement: rapid = 90%, 2 s = 62%, 6 s = 86%, 13 s = 86%, 26 s = 100%

Dental arch: lower arch (Quadrants III and IV) = 81%, upper arch (Quadrants I and II) = 75%.

The tilting and nodding of I, Z and M on a 2-s duration did not cause artefacts in 94% and 88% of cases, respectively. The displacement of I, Z and M by 0.5 and 1.3 mm did not cause artefacts in 100% and 94% of cases, respectively.

Severity

Overall, in all quadrants and anatomic landmarks, the severity index G0, G1, G2 and G3 was present in 52%, 23%, 14% and 11% of cases, respectively.

The artefacts manifesting with vertical X-ray beam had higher prevalence of severity index with respect to those with horizontal X-ray beam: G1 28% *vs* 24%, G2 20% *vs* 10%, G3 10% *vs* 3%.

Table 2. Artefacts prevalence, by severity index, in the four quadrants with horizontal and vertical X-ray beam, with rapid and short duration movements (combined)

Severity index	90° rapid + 2 + 6 s				180° rapid + 2 + 6 s				270° rapid + 2 + 6 s			
	I (%)	II (%)	III (%)	IV (%)	I (%)	II (%)	III (%)	IV (%)	I (%)	II (%)	III (%)	IV (%)
G0	78.6	37.5	40.5	86.9	37.5	48.2	52.7	27.7	48.8	73.8	82.1	39.3
G1	16.7	34.8	34.5	11.9	34.8	27.6	20.5	29.5	32.1	19.0	16.7	33.3
G2	4.7	17.8	17.9	1.2	17.8	13.5	17.9	31.2	13.1	7.2	1.2	20.2
G3	0	9.9	7.1	0	9.9	10.7	8.9	11.6	6	0	0	7.2
Total	100	100	100	100	100	100	100	100	100	100	100	100

Area

During the movement with horizontal X-ray beam, the artefacts prevailed in the lower quadrant opposed to the source. With the X-ray source at 90° position, they were in Quadrant III in 60% of cases and in Quadrant IV in 13% of cases, whereas with the X-ray source at 270° position, they were in Quadrant III in 18% of cases and in Quadrant IV in 61% of cases. The evaluation of the source side only showed more artefacts in the upper quadrant with respect to the lower quadrant (21% *vs* 13% on the right, 26% *vs* 18% on the left) (Table 2).

During movement with vertical X-ray beam, the artefacts were nearly symmetrical in case of rapid movements (Quadrant I 82%, Quadrant II 79%, Quadrant III 75%, Quadrant IV 82%), whereas with continuous movement of 2 and 6 s, they showed distinct prevalence in the right (Quadrant I 43%, Quadrant II 25%, Quadrant III 20%, Quadrant IV 63%) (Table 3).

We noticed that artefacts at the incisors' alveoli site were more frequent in case of nodding.

Extension

The true monolateral artefacts were 25%, the false monolateral artefacts were 23% and the bilateral artefacts were 52%. Both true and false monolateral artefacts distinctly prevailed in short-duration movements (rapid + 2 + 6 s = 95% in both cases), with horizontal beam (75% in both cases) and 5-cm displacement (slightly <50% in both cases).

The bilateral artefact was frequent with long-duration movements (13 + 26 s = 40%) and large displacement (10 cm = 49%), with no substantial differences with respect to the beam angle (Table 4).

Type

With rapid movements and with continuous movements of 2 and 6 s, double contour and smearing prevailed, occurring in 58% of cases, whereas the fading of bone trabeculae and the general loss of sharpness and contrast did not occur or were very modest (G0 + G1) in 87% of cases. With 13- and 26-s movements, all types of artefacts occurred in at least 79% of cases, whereas G3 bone trabeculae fading reached the highest prevalence (42%) (Table 5).

DISCUSSION

In this study, small controlled movements of nodding, tilting and rolling were imparted to a dry skull during CBCT examinations, to investigate the basic mechanisms that lead to motion artefacts, which are common in daily practice, and the relationships between the type of movement and type of artefact.

A CBCT system for horizontal (supine) patient positioning was used because the gantry rotates more stably in a vertical plane. Furthermore, the patient-bearing table is not mechanically connected to the machine, which prevents the transfer of vibrations during the rotation of the gantry.[8]

The flat-panel detector of NewTom 5G is offset from the source–rotation centre axis in order to enlarge the reconstructed FOV. In so doing, the peripheral portion of the scanned volume is reconstructed with a lower number of projected images, and

Table 3. Artefacts prevalence, by severity index, in the four quadrants with vertical X-ray beam, with rapid and with short duration movements

Severity index	180° rapid				180° 2 + 6 s			
	I (%)	II (%)	III (%)	IV (%)	I (%)	II (%)	III (%)	IV (%)
G0	17.9	21.4	25.0	17.9	57.1	75.0	80.4	37.5
G1	39.2	35.7	21.4	21.4	30.4	19.6	19.6	37.5
G2	25.0	21.5	35.7	42.8	10.7	5.4	0	19.6
G3	17.9	21.4	17.9	17.9	1.8	0	0	5.4
Total	100	100	100	100	100	100	100	100

Table 4. Percent distribution of the artefacts, by extension, as a function of orientation of the X-ray beam, and the length and duration of the movement

Extension	X-ray beam (%)			Length (cm) (%)				Duration (s) (%)				
	Horizontal	Vertical	Total	2.5	5	10	Total	Rapid	2	6	13	26	Total
True monolateral	75.2	24.8	100	26.9	49.2	23.9	100	28.6	25.0	41.6	4.8	0	100
False monolateral	74.7	25.3	100	20.0	46.2	33.8	100	35.4	22.8	36.7	5.1	0	100
Bilateral	53.8	46.2	100	17.3	34.0	48.7	100	24.7	16.3	18.5	24.7	15.8	100
True monolateral	35.1	21.8		31.6	28.9	14.4		25.0	30.9	36.1	7.7	0	
False monolateral	32.2	21.8		22.8	26.4	19.8		29.2	26.5	29.9	7.7	0	
Bilateral	32.7	56.4		45.6	44.7	65.8		45.8	42.6	34.0	84.6	100	
Total	100	100		100	100	100		100	100	100	100	100	

only the central portion is based over the total number of images from a full 360° rotation.[5,11] In CBCT, each angular projection contributes in the same way to the development of the volumetric data sets, and the complete object reconstruction is already acquired by images obtained on a rotation of 180° plus an angle corresponding to the X-ray beam aperture.

Spin-Neto et al[7] had imparted direct macroscopic movements (15% in nodding and tilting) with a "robot skull", thus always obtaining artefacts in 100% of cases. He had not effected tiny movements. Conversely, we have moved the skull phantom with a long rigid pole. In doing so, and bringing the fulcrum close to the skull phantom, it was easy to produce small movements, even sub-millimetre, manoeuvring at a distance of 2 m. This made possible to simulate movements as *in vivo*, since the skull phantom rested directly on the same support used for a live patient.

Not all movements that we have imparted resulted in artefacts affecting a visual evaluation of the images. In fact, no artefacts were detected when the movement was so small that the anatomical landmarks were not reconstructed at discernibly separate locations, or when the number of images acquired during the movement was so small that they did not significantly contribute to the reconstruction of that anatomical detail, contributing instead to an increase of the background noise. This occurred with movements of I, Z and M of 0.5 mm in 100% of cases, of 1.3 mm in 94% of cases and 2-s tilting movements in 94% of cases.

In our selection of movements, the one that caused the maximum prevalence of artefacts was rolling (100%). The different prevalence of artefacts between nodding (92%) and tilting (67%) is due to the different displacement of the anatomical structures in the two types of movement, at equal pole displacement, depending upon the position of the fulcrum. In fact, the artefacts prevailed in the lower quadrant, as opposed the upper quadrants, with M > Z > I in case of tilting and I > Z > M in case of nodding.

The location where the artefacts manifested themselves depended upon the acquisition angle and the offset between the X-ray beam and the centre of the detector. This may be caused by the projection geometry of the two-dimensional images acquired; we speculate that, perhaps, the anatomical structures farer away from the detector may contribute to the reconstruction of the volumetric data set to a lesser extent than others, because of the greater discrepancy from the ideal back-projection geometry and/or to their greater enlargement. This could also explain why the artefacts were visible in all the quadrants when the X-ray beam was vertical, whereas they may have been visible in a single quadrant or in crossed quadrants (I and III, or II and IV) when the X-ray beam was horizontal.

The extent of the artefacts depended mainly on the duration of the movement and was affected by the position of the X-ray source and the pole displacement. In CBCT, owing to the long rotation time of the gantry, the images acquired during rapid or short-duration movements (2 and 6 s) are few (1–23%). This caused the formation of artefacts on a single side (Figure 4) or part of it (short artefacts) (Figure 5) when the X-ray source was

Table 5. Prevalence of the artefacts, by severity index—smearing (S), double contour (D), loss of visibility of bone trabeculae (T) and general spatial unsharpness (U)—as a function of the movement duration

Severity index	Rapid (%)				2–6 s (%)				13–26 s (%)			
	S	D	T	U	S	D	T	U	S	D	T	U
0	25.0	25.0	45.2	36.9	58.3	61.9	80.4	76.8	15.5	19.0	19.0	21.4
1	36.9	22.6	35.7	39.3	24.4	29.2	14.8	18.5	20.2	27.4	11.9	16.7
2	25.0	25.0	14.3	16.7	13.7	7.1	4.8	4.7	28.6	32.2	27.4	32.1
3	13.1	27.4	4.8	7.1	3.6	1.8	0.0	0.0	35.7	21.4	41.7	29.8
Total	100.0	100.0	100.0	100.0	100.0	100.0	100.0	100.0	100.0	100.0	100.0	100.0

horizontal, and with artefacts present exclusively or prevailingly in one side (true monolateral and false monolateral artefacts, respectively). Conversely, with movements of duration equal to or larger than a half of the rotation time (13 and 26 s), the artefacts extended upon both sides with no significant differences (bilateral artefacts) (Figures 6 and 7).

The double contour artefacts were more evident with rapid movements (G3 = 27.4%) than with continuous movements, because two distinct sets of images were acquired. In each set, the anatomical points did not change the relative positions, but each set was displaced with respect to the other, the distance between the two contours being determined by the extent of the displacement. Conversely, in case of continuous movements, the same point was acquired in a gradually changing position, and the final images were reconstructed with a smearing that was especially noticeable with movements of 2 and 6 s (42%). The intensity and thickness of the smearing were proportional to the duration and the extent of the movement, respectively.

The fading of bone trabeculae and the general loss of spatial resolution and contrast (unsharpness) reached the highest prevalence in movements of 13 and 26 s (80%), being caused by the combined effect of smearing and double contours. Furthermore, the general loss of spatial resolution and contrast, which in our opinion is the artefact that affects more severely the diagnostic quality of the images, is the one with the lowest prevalence of G3 (12%). This may explain what is reported in other works,[2,3,6] where it was diagnostically necessary to repeat the examination only in 0.5%, 1.9% and 0.4%, respectively, of cases where motion artefacts were present.

We have noticed that the artefact follows the direction of the movement: in nodding it was more evident in the craniocaudal direction (Figure 6), whereas in tilting and rolling, it was in the lingual–vestibular direction (Figure 7).

A limit of our study is that we have imparted the movement manually, rather than mechanically/automatically. However, operators' coaching and practicing to consistently reproduce the movements, the use of a chronometer and a metronome for the timing, and end stops to precisely determine the displacement, rendered the imparted movements quite reproducible. Another limit is that we have not considered all the possible types of movement, especially the combined ones (nodding, tilting and rolling simultaneously) which are more complicated and closer to the actual movements of a live patient. Furthermore, we did not consider the movement of the mandible alone, which is the only independently mobile bone of the maxillofacial complex. Instead, we have performed many elementary movements to establish which are the most relevant ones in producing artefacts and to identify them from the artefact's features. This helped assessing the diagnostic validity of images that are partly degraded by artefacts, thus reducing unnecessary retakes. The current European guidelines state that a maximum of 5% of all CBCT examinations could be considered diagnostically unacceptable and require a retake.[18]

In order to reduce the occurrence of motion artefacts, further studies may be helpful at evaluating the various methods available for skull immobilization, and develop software for mathematical algorithms that identify and remove images acquired during patient movements to improve the quality of the reconstructed data set and reduce the need of retakes and additional radiation dose to patient.

These results were obtained with a specific model of CBCT, with supine patient position. Different specific results might be found with CBCT systems that use another patient-positioning approach (sitting or standing), faster scan times, detectors of different size and with no offset, other rotation modes and other 3D reconstruction algorithms. In particular, we think that devices with very fast speed rotation (5–10 s) could reduce smearing and general unsharpness. However, the general conclusions reached here should apply to the generality of dento-maxillofacial CBCT systems, since the fundamental physical principles of 3D reconstruction are common to all.

CONCLUSION

Our study has made possible to recognize the different types of motion artefacts and to correlate them with the causing types of patient movement, thus reducing the chance of attributing to other reasons the degraded image features.

The main cause of artefacts, which can occur in all quadrants (bilateral), in one quadrant only (monolateral) or even in part of it (monolateral short artefacts) is rolling (100%), followed by nodding (92%) and tilting (67%).

Rapid and short-duration (2 and 6 s) movements mostly caused double contour and smearing, whereas the long duration movements (13 and 26 s) caused loss of trabeculae visibility and general unsharpness. Movements of very small extension did not produce visible artefacts (0.5 mm in 100% of cases and 1.3 mm in 94% of cases).

REFERENCES

1. Nemtoi A, Czink C, Haba D, Gahleitner A. Cone beam CT: a current overview of devices. *Dentomaxillofac Radiol* 2013; **42**: 20120443. doi: 10.1259/dmfr.20120443
2. Spin-Neto R, Matzen LH, Schropp L, Gotfredsen E, Wenzel A. Factors affecting patient movement and re-exposure in cone beam computed tomography examination. *Oral Surg Oral Med Oral Pathol Oral Radiol* 2015; **119**: 572–8. doi: 0.1016/j.oooo.2015.01.011
3. Nardi C, Borri C, Regini F, Calistri L, Castellani A, Lorini C, et al. Metal and motion artifacts by cone beam computed tomography (CBCT) in dental and maxillofacial study. *Radiol Med* 2015; **120**: 618–26. doi: 10.1007/s11547-015-0496-2
4. Holberg C, Steinhäuser S, Geis P, Rudzki-Janson I. Cone beam computed tomography in orthodontics: benefits and limitations. *J Orofac Orthop* 2005; **66**: 434–44. doi: 10.1007/s00056-005-0519-z
5. Schulze R, Heil U, Groß D, Bruellmann DD, Dranischnikow E, Schwanecke U, et al. Artefacts in CBCT: a review. *Dentomaxillofac Radiol* 2011; **40**: 265–73. doi: 10.1259/dmfr/30642039
6. Donaldson K, O'Connor S, Heath N. Dental cone beam CT image quality possibly reduced by patient movement. *Dentomaxillofac Radiol* 2013; **42**: 91866873. doi: 10.1259/dmfr/91866873
7. Spin-Neto R, Mudrak J, Matzen LH, Christensen J, Gotfredsen E, Wenzel A. Cone beam CT image artefacts related to head motion simulated by a robot skull: visual characteristics and impact on image quality. *Dentomaxillofac Radiol* 2013; **42**: 32310645. doi: 10.1259/dmfr/32310645
8. Hanzelka T, Dusek J, Ocasek F, Kucera J, Sedy J, Benes J, et al. Movement of the patient and the cone beam computed tomography scanner: objectives and possible solutions. *Oral Surg Oral Med Oral Pathol Oral Radiol* 2013; **116**: 769–73. doi: 10.1016/j.oooo.2013.08.010
9. Spin-Neto R, Matzen LH, Schropp L, Liedke GS, Gotfredsen E, Wenzel A. Radiographic observers' ability to recognize patient movement during cone beam CT. *Dentomaxillofac Radiol* 2014; **43**: 20130449. doi: 10.1259/dmfr.20130449
10. Schulze RK, Michel M, Schwanecke U. Automated detection of patient movement during a CBCT scan based on the projection data. *Oral Surg Oral Med Oral Pathol Oral Radiol* 2015; **119**: 468–72. doi: 10.1016/j.oooo.2014.12.008
11. Molteni R. Prospects and challenges of rendering tissue density in Hounsfield units for cone beam computed tomography. *Oral Surg Oral Med Oral Pathol Oral Radiol* 2013; **116**: 105–19. doi: 10.1016/j.oooo.2013.04.013
12. Feldkamp LA, Davis LC, Kress JW. Practical cone-beam algorithm. *J Opt Soc Am* 1984; **1**: 612–19. doi: 10.1364/JOSAA.1.000612
13. Sharp GC, Kandasamy N, Singh H, Folkert M. GPU-based streaming architectures for fast cone-beam CT image reconstruction and demons deformable registration. *Phys Med Biol* 2007; **52**: 5771–83. doi: 10.1088/0031-9155/52/19/003
14. Katsumata A, Hirukawa A, Noujeim M, Okumura S, Naitoh M, Fujishita M, et al. Image artifact in dental cone-beam CT. *Oral Surg Oral Med Oral Pathol Oral Radiol Endod* 2006; **101**: 652–7. doi: 10.1016/j.tripleo.2005.07.027
15. Braun H, Kyriakou Y, Kachelriess M, Kalender WA. The influence of the heel effect in cone-beam computed tomography: artefacts in standard and novel geometries and their correction. *Phys Med Biol* 2010; **55**: 6005–21. doi: 10.1088/0031-9155/55/19/024
16. Schulze RK, Berndt D, d'Hoedt B. On cone-beam computed tomography artefacts induced by titanium implants. *Clin Oral Implants Res* 2010; **21**: 100–7. doi: 10.1111/j.1600-0501.2009.01817.x
17. Chindasombatjareon J, Kakimoto N, Murakami S, Maeda Y, Furukawa S. Quantitative analysis of metallic artefacts caused by dental metals: comparison of cone-beam and multi detector row CT scanners. *Oral Radiol* 2011; **27**: 114–20.
18. SEDENTEXCT Project. *Radiation protection n°172: cone beam CT for dental and maxillofacial radiology*. Luxembourg: European Commission Directorate-General for Energy; 2012.